Differentiation trend and parent melt composition of Ni-bearing gabbro-wehrlite Pechenga intrusions, Kola Peninsula

Article *in* Petrology · July 2001

CITATIONS
7

READS
61

3 authors, including:

Rais Latypov
University of the Witwatersrand
107 PUBLICATIONS **1,009** CITATIONS

SEE PROFILE

Petrology, Vol. 9, No. 4, 2001, pp. 329–344. Translated from Petrologiya, Vol. 9, No. 4, 2001, pp. 381–397.

Differentiation Trend and Parent Melt Composition of Ni-Bearing Gabbro–Wehrlite Pechenga Intrusions, Kola Peninsula

R. M. Latypov*, [1], V. F. Smolkin*, and T. T. Alapieti**

** Geological Institute, Kola Research Center, Russian Academy of Sciences, ul. Fersmana 14, Apatity, Murmansk oblast, 184200 Russia*

*** Institute of Geosciences, University of Oulu, FIN-90401, Oulu, Finland*
e-mail: Rais.Latypov@oulu.fi

Received November 11, 2000

Abstract—The geologic section of the widely known Pechenga intrusions with accompanying nickeliferous mineralization consists of the following three principal zones (listed in order from bottom to top): wehrlite, clinopyroxenite, and gabbro. It is commonly believed that this succession of zones corresponds to the following crystallization sequence of silicates: *Ol* ⟶ *Ol + Cpx* ⟶ *Cpx + Pl* (Smolkin, 1974, 1977a; Marakushev *et al.*, 1986; Hanski, 1992). This crystallization succession implies olivine disappearance in the absence of peritectic reactions between olivine and any of the phases. To settle this problem, we performed an additional petrological investigation of the Pilgujarvi intrusion, the largest in the Pechenga group, in which relict primary magmatic assemblages are preserved. The rocks of the gabbro zone were determined to pervasively contain serpentine–chlorite pseudomorphs after olivine, a fact suggesting that olivine crystallization did not stop in the upper portion of the intrusion. Hence, the actual differentiation trend of the nickeliferous Pechenga intrusions corresponds to one of the theoretically possible crystallization trends of basaltic magma within the volume of the *Ol–Cpx–Pl–Qtz* phase diagram: *Ol* ⟶ *Ol + Cpx* ⟶ *Ol + Cpx + Pl* (Irvine, 1970). The composition of the parent melt of nickeliferous intrusions is traditionally inferred from the weighted mean composition of the intrusion or the composition of its lower chill zones. However, practically all of the intrusive rocks were metamorphosed under greenstone-facies conditions, and, hence, the direct use of their chemical analyses faces certain obstacles. The best compatibility with the established differentiation trend is shown by the compositions calculated from the quantitative mineralogical compositions of the rocks and the actual chemistry of their rock-forming, accessory, and ore minerals.

INTRODUCTION

The nickeliferous Pechenga intrusions affiliate with the Early Proterozoic gabbro–wehrlite association of the Fennoscandian (Baltic) Shield (Smolkin, 1977b; *Magmaticheskie…*, 1979). The close attention arrested by these intrusions is caused by the fact that they are accompanied by a series of large (economic) Cu–Ni deposits (*Mednonikelevye…*, 1985; *Medno-nikelevye…*, 1999). Several of the nickeliferous intrusions display a clearly primary differentiated inner structure. They consist of three principal zones (from bottom to top: wehrlite, clinopyroxenite, and gabbro) and chill zones (Eliseev *et al.*, 1961; Smolkin, 1974, 1977a). Undifferentiated intrusions are made up of wehrlite, wehrlite and clinopyroxenite, or, more rarely, gabbroids. A realistic model for the genesis of the mineral deposits can be developed based on the following information: (1) the composition of the parental melt, which contained ore-forming components and (2) the crystallization trend of this melt in a magmatic chamber. The composition of the parental melt can be either inferred from the compositions of chill zones or calculated based on the weighted mean compositions of all zones of one or several intrusions. The crystallization trend is deduced from the crystallization succession of cumulus phases in the stratigraphic section of the intrusion. However, the intrusive rocks were affected by metamorphic alterations under greenschist-facies conditions, and, thus, it is difficult to reproduce their original modal and chemical composition, which, in turn, may lead to contradictory conclusions.

One of the contradictions concerns inconsistencies in the crystallization order of silicate minerals in the Pechenga intrusions, a fact that we discovered based on petrographic observations and their comparison with the crystallization order that can be deduced from the physicochemical analysis of the parental melt of the intrusions. It is commonly admitted that the succession of zones in the Pechenga intrusions provide evidence of the following crystallization order of silicate phases: *Ol* ⟶ *Ol + Cpx* ⟶ *Cpx + Pl* (Eliseev *et al.*, 1961; Smolkin, 1974, 1977a; Hanski, 1992).[2] This implies the disap-

[1] Present address: Institute of Geosciences, University of Oulu, P.O. Box 3000, FIN-90401 Oulu, Finland.

[2] In the text, tables, and figures below, the following abbreviations are used: *Pl*—plagioclase, *Ol*—olivine, *Opx*—orthopyroxene, *Cpx*—clinopyroxene, *Qtz*—quartz, *f*# = Fe/(Fe + Mg) for the Fe mole fraction of mafic minerals, *An* = 100 × *An*/(*An* + *Ab*) for plagioclase number, *Cal*—calcite, *Ap*—apatite, *Ilm*—ilmenite, *Mag*—magnetite, *Hem*—hematite, *Chr*—chromite, *Py*—pyrite, *Or*—orthoclase, *Ab*—albite, *An*—anorthite, *Ne*—nepheline, *En*—enstatite, *Fs*—ferrosilite, *Di*—diopside, *Hd*—hedenbergite, *Fo*—forsterite, *Fa*—fayalite, *L*—melt, $an^L = 100 \times An/(An + Ab)$ for the normative composition of plagioclase in melt, f_L = Fe/(Fe + Mg) for the Fe mole fraction of melt, $Ol_{25–50}$—olivine and the interval of its Fe mole fraction, $Pl_{60–70}$—plagioclase the interval of its Ca mole fraction.

pearance of liquidus olivine from the rocks of the gabbro zone. However, olivine cannot disappear from the liquidus until the termination of melt crystallization unless it becomes involved in a peritectic reaction with some phase. According to the topology of the *Fo–Di–An* phase diagram (Osborn and Tait, 1952), which describes (in a simplified form) the composition of the parental melt of the Pechenga intrusions, olivine cannot disappear due to peritectic reactions. All melt compositions of this system should end their crystallization at the eutectic point with the three-phase assemblage (*Ol + Cpx + Pl*) of olivine gabbro. Hence, petrographic observations come in conflict with the theory of crystallization differentiation. The aim of this study was to resolve this contradiction.

GEOLOGICAL OVERVIEW AND CHARACTERIZATION OF GABBRO–WEHRLITE INTRUSIONS

The Pechenga structure that hosts the nickeliferous gabbro–wehrlite intrusions is located in the north of the Fennoscandian Shield, in the northwestern part of the Kola Peninsula, within the Murmansk oblast (province) of Russia (Fig. 1). The structure is one of the most thoroughly studied geologic bodies of the area because of associated economic deposits of Cu–Ni sulfide mineralization and works at the Kola Superdeep Hole (*Medno-nikelevye…*, 1985; Smolkin *et al.*, 1995; *Magmatizm…*, 1995; *Seismologicheskaya model'…*, 1997; *Kol'skaya sverkhglubokaya*, 1998; *Medno-nikelevye…*, 1999).

Steep faults divide the structure into two tectono–stratigraphic units, the Northern Pechenga and Southern Pechenga zones (Fig. 1), which differ in stratigraphy, styles of tectonics, and rock ages. The Northern Pechenga Zone consists of alternating volcanic and sedimentary rocks of the Early Karelian Complex, which compose a northeast-dipping monoclinal rock sequence 8.5 km thick. The composition of the volcanic rocks and comagmatic dikes and sills ranges from basaltic andesite and dacite to trachybasalt and, then, tholeiitic basalt and ferropicrite. The rocks are metamorphosed to the greenschist and amphibolite facies. The Southern Pechenga Zone hosts high-grade, deformed metamorphic rocks, which were transformed into amphibolites, schists, and gneisses (including garnet-bearing varieties) with an overall thickness up to 3.5 km. The reconstructed composition of the volcanic and subvolcanic rocks varies from basalt and picrite to basaltic andesite, andesite, dacite, and rhyolite.

Both Ni-bearing intrusions and sills of ophitic gabbro are located in the central part of the Northern Pechenga Zone, predominantly among the tuff–sedimentary (so-called producing) member (Zhdanovskaya Formation), or, more rarely, are hosted by the underlying volcanic deposits of the Zapolyarninskaya Formation (Fig. 1). Some of the intrusions (Kaula, Kotselvaara, Kammukivi, Kierdzhipori, Severnyi, and Pilgujarvi) are accompanied by economic deposits of Cu–Ni massive, brecciated, high-grade disseminated, or disseminated sulfide ores (*Medno-nikelevye…*, 1999). The intrusions are laccolith-, phacolith-shaped, or, more rarely, cutting bodies, whose thicknesses vary from a few dozen to 600 m and which extend for 50–100 to 6000 m. Some of them can be traced for 2500 m down the dips. The nickeliferous intrusions most often have a differentiated inner structure or, more rarely, are relatively homogeneous and consist of serpentinite or gabbro. The stratigraphic bottoms of the differentiated intrusions are composed of olivine cumulates (wehrlites), which grade upsection into olivine–clinopyroxene, titanomagnetite–olivine, and clinopyroxene cumulates and, further upward, give way to plagioclase–clinopyroxene cumulates (gabbro). The intrusive rocks and host schists were metamorphosed to the greenschist facies in the central part of the structure and amphibolite facies in its flanks and underwent extensive metasomatic alterations (are replaced by chlorite, talc, and carbonates) within orebodies.

INNER STRUCTURE, CUMULUS STRATIGRAPHY, AND COMPOSITION OF INTRUSIONS

The ore field includes more than 300 Ni-bearing intrusions. The active metamorphic transformations and structural–tectonic deformations of most of these intrusions made them little suitable for the resolution of the problems formulated above. For our study, we selected one of the largest bodies, the Pilgujarvi intrusion, whose rocks largely retain their original fabrics and composition. The intrusion hosts the large, economic Zhdanovskoe deposit of Cu–Ni ores, which is exposed by open-cast and underground mines (*Medno-nikelevye…*, 1999) and, hence, became a testing ground for studying the genesis of rocks and ore mineralization in this ore field. The most exhaustive materials on the inner structure of this intrusion and the mineralogy and geochemistry of its rocks were published by Smolkin (1974, 1977a, 1978), Zak *et al.* (1982), Smolkin and Pachomovskiy (1985), Marakushev *et al.* (1986), and Hanski (1992) and were presented in the monographs *Magmatism…* (1995) and *Medno-nikelevye…* (1999). The U–Pb zircon and baddeleyite age of the gabbro is 1982 ± 8 Ma (Smolkin and Bayanova, 1999).

The Pulgujarvi intrusion consists of a series of large blocks separated by faults. The most complete geologic section can be examined in the so-called Glavnyi Massif, which is a concordant intrusion, trending for 2200 m northwestward and dipping southwestward at angles of 45°–55° (Fig. 2). The massif was traced for depths of more than 2000 m, until which it does not exhibit any traces of tapering. The thickness of the intrusion varies from 300 to 500 m. It has a sheet- and bowl-shaped longitudinal and transverse cross-sections, respectively, and is truncated by steep faults in flanks. The intrusive is generally conformable with the

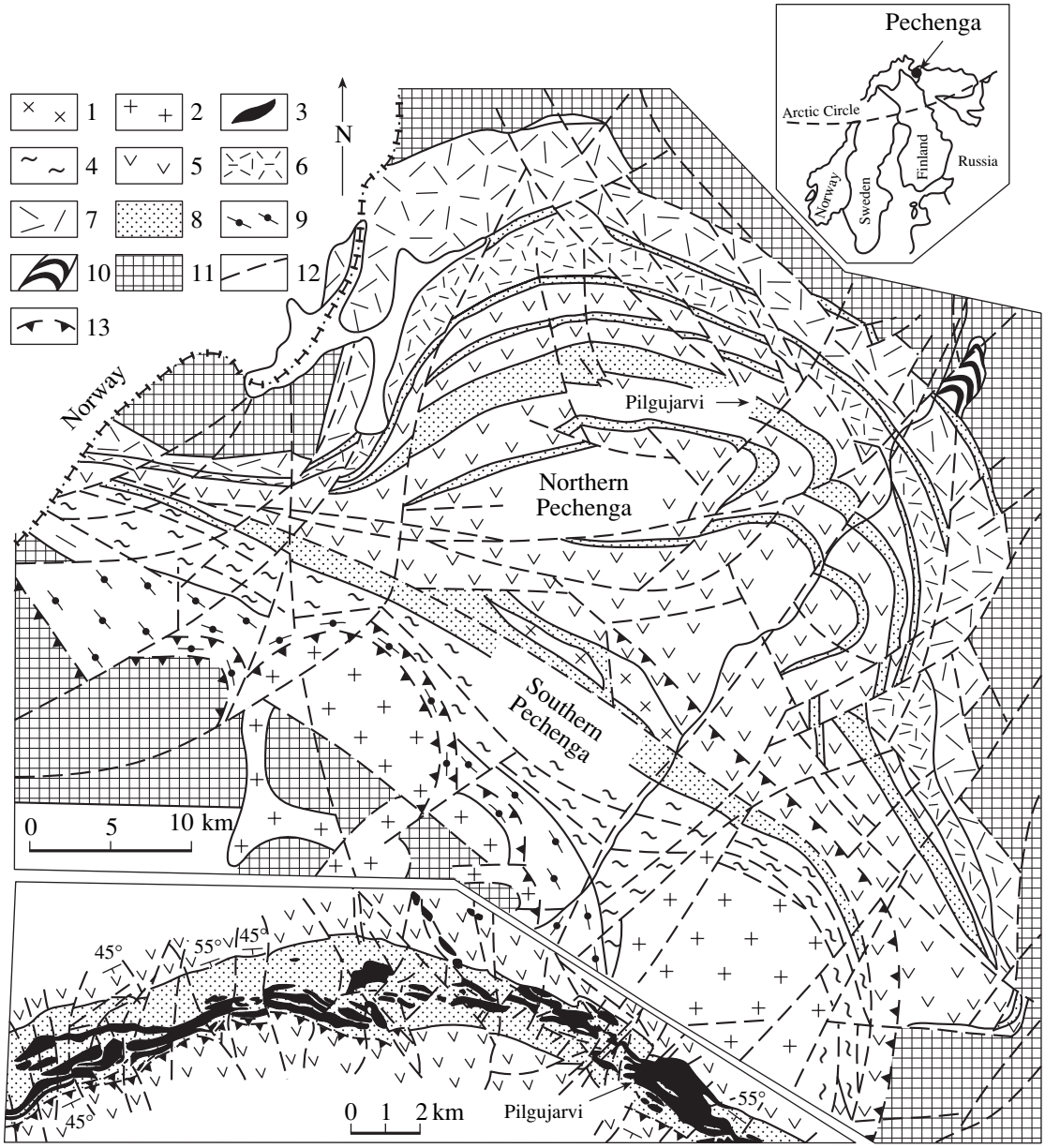

Fig. 1. Schematic geological map of the Pechenga area. The inset shows the position of gabbro–wehrlite Ni-bearing intrusions (modified after *Magmatizm…*, 1995).

(1) Dacite and rhyolite of the Poritash subvolcanic complex; (2) granite and granodiorite; (3) Ni-bearing gabbro–wehrlite intrusions; (4) schists, metavolcanics of basaltic, picritic, andesitic, and rhyolitic composition, and their tuffs; (5) tholeiitic basalt, ferropicrite, and their tuffs; (6) trachybasalt, trachybasaltic andesite, trachyte, and basalt; (7) basaltic andesite and dacite; (8) conglomerate, gritstone, quartzite, dolomite, tuffs, and schists; (9) garnet gneisses and amphibolites, schistose amphibolites; (10) gabbronorite of the Mt. General'skaya layered intrusion; (11) Archean complex of gneisses, amphibolites, and migmatites; (12) steep faults; (13) gently dipping faults.

country rocks but sometimes shows cross-cutting relationships with earlier sills of ophitic gabbro.

The generalized geologic section of the Glavnyi Massif consists of (Smolkin, 1974, 1977a) a lower and an upper marginal (chill) zone, wehrlite (more specifically, wehrlite–olivinite) zone, transitional (critical) zones, a gabbro–pyroxenite zone, and a zone of pegmatoid gabbro (Figs. 2, 3). For simplicity sake, the latter two zones are not shown in Fig. 3 separately but denoted as a single gabbro zone.

The wehrlite zone has an average thickness of approximately 135 m and is dominated by serpentinized wehrlite (<75 vol % *Ol*) and mineralized or barren serpentinite, which contains lenticular strata of pyroxene-rich olivinite (>75 vol % *Ol*). The cumulus minerals of the rocks of this zone are serpentinized oli-

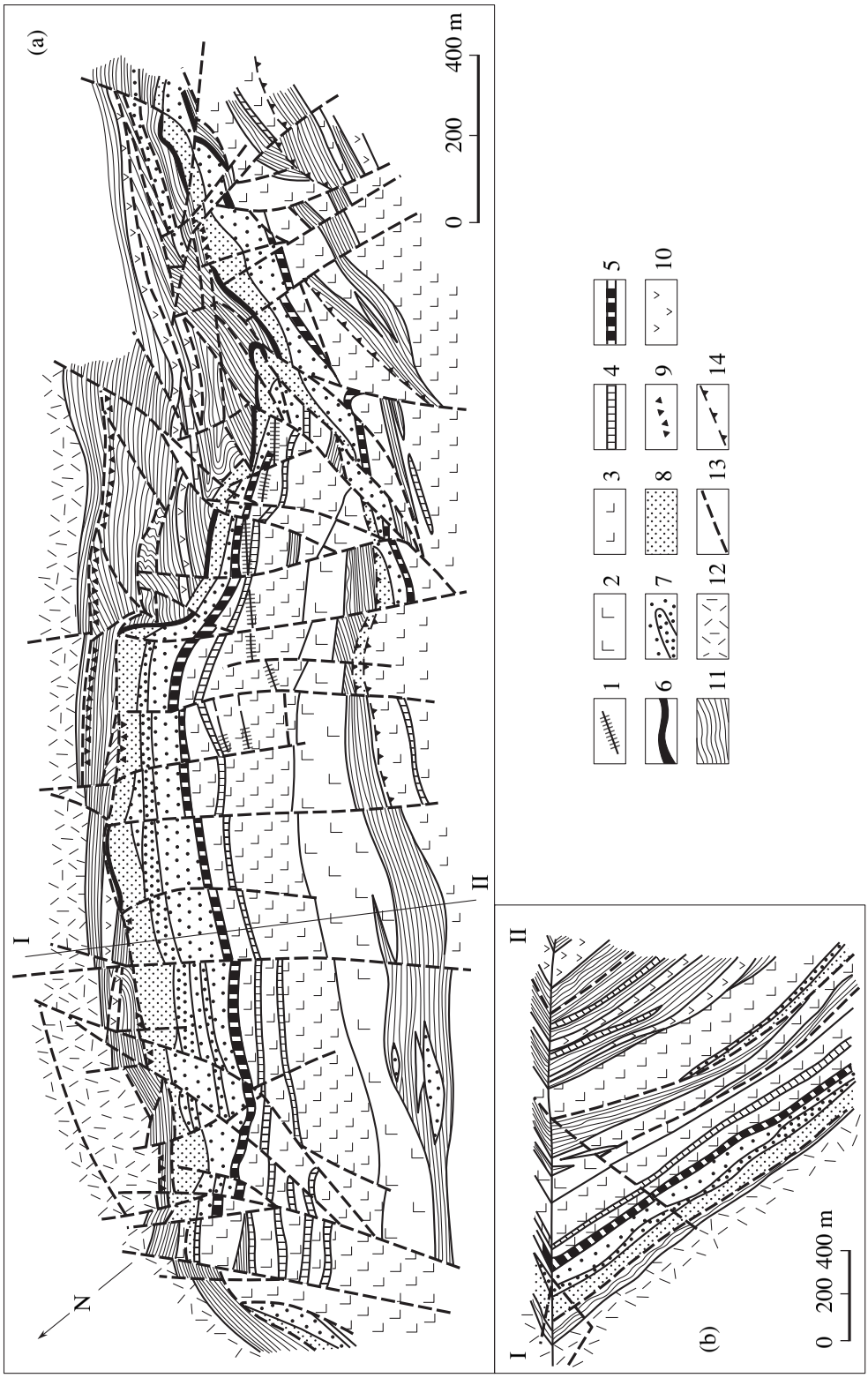

Fig. 2. Pilgujarvi intrusion: (a) schematic geological map and (b) geological cross section (simplified after Smolkin, 1977a). (1) Dolerite dikes; (2) orthoclase gabbro; (3) gabbro; (4) plagioclase pyroxenite of the gabbro zone; (5) rocks of the transitional unit; (6) clinopyroxenite of the marginal zone; (7) wehrlite with lenses of olivinite rich in pyroxene; (8) wehrlite with disseminated sulfide mineralization; (9) brecciated sulfide mineralization; (10) pillow and massive tholeiitic lavas of the Zapolyarninskaya Formation; (11) host schists; (12) tholeiitic lavas and their tuffs of the Matert Formation; (13) faults; (14) reversed and thrust faults. I–II line of the geological profile shown in the inset.

vine (chrysolite) and Cr-spinel (Ti-chromite), and the intercumulus phases are clinopyroxene (Ti-augite), amphibole (kaersutite), and Ti-biotite. The rocks occasionally contain relics of intercumulus plagioclase, which is replaced by chlorite. The clinopyroxene develops in the form of phenocrysts with poikilitic olivine inclusions.

The transitional (critical) unit has a thickness of 8–16 m and consists (from bottom to top) of fine-grained olivine-bearing clinopyroxenite, titanomagnetite olivinite, and titanomagnetite plagioclase pyroxenite. The unit is characterized by the first appearance of cumulus clinopyroxene and titanomagnetite. The overall concentration of cumulus olivine decreases to 10–20 vol %. The intercumulus phases are kaersutite, Ti-biotite, and plagioclase.

The gabbro zone has a thickness of 300 m and accounts for more than two-thirds of the total massif volume. Upsection, melano- and mesocratic gabbro with plagioclase pyroxenite layers give way to mesocratic gabbro with pronounced trachytoid structures and, further upward, to pegmatoid and orthoclase-bearing gabbro with massive or taxitic structures. The lower boundary of the gabbro zone is drawn based on the first appearance of cumulus plagioclase and the disappearance of olivine. The cumulus minerals are plagioclase, clinopyroxene (Ti-augite), titanomagnetite, and ilmenite. The intercumulus material contains kaersutite and Ti-biotite. Potassic feldspar develops as antiperthitic rims around plagioclase crystals in gabbroids of the apical portion of the massif.

The analysis of variations in the rock chemistry over the geologic section (Fig. 4, Table 1) led us to reveal clearly pronounced cryptic layering. For example, the normative number of plagioclase systematically and continuously decreases upsection, simultaneously with an increase in the partial Fe#, which is highly consistent with the principle of mafic magma fractional differentiation. It is interesting to consider the diagram (Fig. 5) demonstrating a negative correlation between the normative composition of the plagioclase and its concentration in the rocks. As follows from the *Ab–An–Di* phase diagram topology, this tendency is controlled by the systematic changes in the cotectic relations between plagioclase and mafic minerals in the course of magmatic differentiation.

At the same time, it is worth mentioning the apparent gap between the wehrlite and gabbro zones in terms of the normative pyroxene ratio (Fig. 4, *K*(*hy*)). A rapid increase in this ratio within the wehrlite zone was caused by the occurrence of significant amounts of normative orthopyroxene (up to 50%) and plagioclase (up to 20%) at an insignificant concentration of clinopyroxene (<5%). In fact, the normative composition of the rocks corresponds to plagioclase harzburgite, and this suggests that the rocks probably contain modal orthopyroxene. However, the detailed petrographic examination of the rocks did not reveal either primary orthopyroxene or pseudomorphs of secondary minerals after it. Hence, the appearance of normative orthopyroxene may have been caused by the allochemical character of metamorphic transformations in the rocks of the wehrlite zone (Smolkin, 1992). The origin of normative orthopyroxene is coupled with the replacement of olivine by serpentine, talc, and chlorite, which always contain significant amounts of orthopyroxene end-members. The production of normative orthopyroxene at the expense of olivine during metamorphic transformations is confirmed by a positive correlation between the normative pyroxene ratio, *K*(*hy*), and the loss on ignition, LOI (Fig. 4).

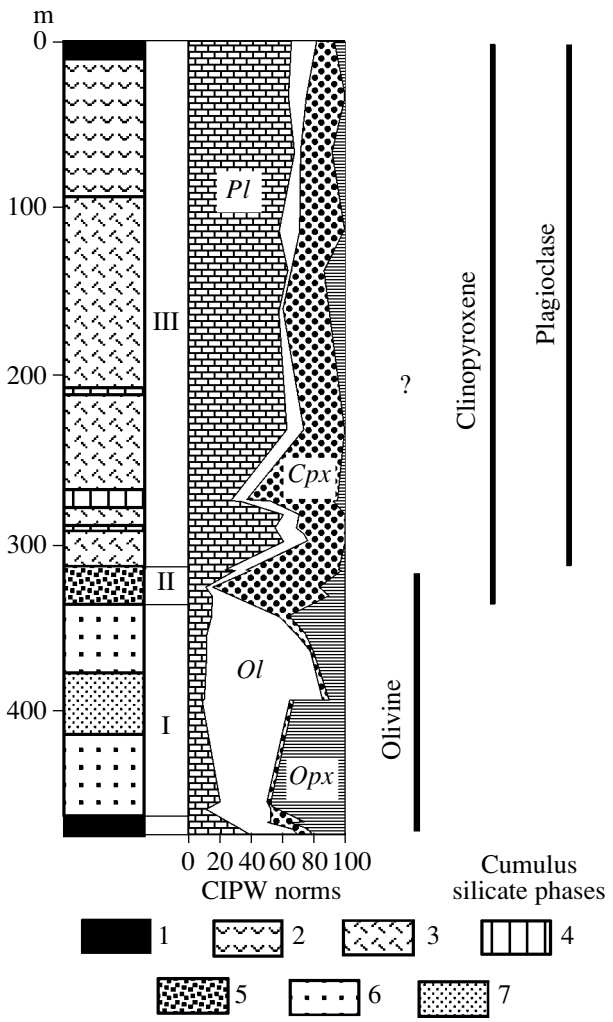

Fig. 3. Generalized vertical section of the Pilgujarvi intrusion.

(1) Clinopyroxenite of the marginal zone; (2) orthoclase gabbro; (3) gabbro; (4) plagioclase pyroxenite; (5) olivine and plagioclase pyroxenite, titanomagnetite olivinite; (6) wehrlite; (7) olivinite enriched in pyroxene; (I) wehrlite zone; (II) transitional (critical) unit; (III) gabbro zone. The column with normative-composition variations is based on the data of Table 1.

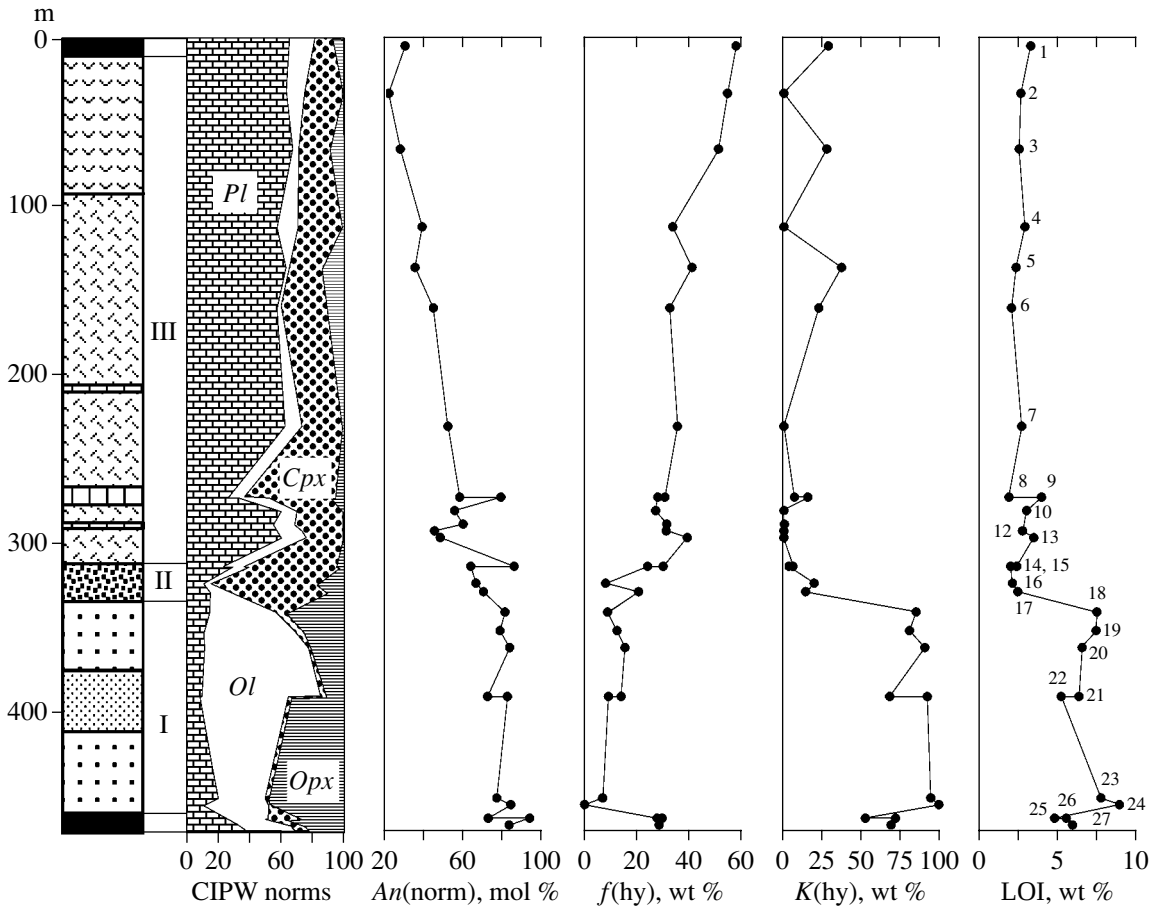

Fig. 4. Variations in rock composition in the cross section of the Pilgujarvi intrusion.
An(norm) = 100 × *An*/(*An* + *Ab*), *f*(hy) = 100 × *fs*/(*fs* + *en*), *K*(hy) = 100 × *Opx*/(*Opx* + *Cpx*), LOI is loss on ignition. See Fig. 3 for symbol explanations. Here and in Figs. 5 and 6, the numbers of points correspond to the numbers of samples in Table 1.

DISCUSSION

Reconstruction of the Fractionation Trend of the Pechenga Gabbro–Wehrlite Intrusions: An Example of the Pilgujarvi Mineralized Intrusion

Figure 4 demonstrates that the transition from the wehrlite zone to the transitional unit and further to the gabbro zone is coupled with the disappearance of normative olivine. Although its concentrations in the rocks of the latter two units dramatically diminish, they never fall below 5–10%. In all instances when the olivine content decreases (sometimes to 0.2–0.6%), this is counterbalanced by the corresponding increase in the concentration of normative orthopyroxene. This provides good reasons to think that the rocks of the gabbro zone should contain either olivine itself or some other phase that includes olivine end-members. This conclusion is compatible with the arrangement of the composition points of the rocks in the (*Ol* + *Opx*)–*Cpx*–*Pl* join (Fig. 6): the points compose three swarms, which correspond to the rocks of the wehrlite zone, transitional unit, and gabbro zone. The plagioclase pyroxenites of the gabbro zone (8 and 9) compose group II of the points. The points of the lower (25, 26, and 27) and upper (1) marginal zones are plotted away from the rest of the points. The group I of the points evidently corresponds to the stage of melt crystallization within the olivine field, group II was formed at the olivine–clinopyroxene cotectic, and group III, corresponding to gabbroids (plagioclase–clinopyroxene cumulates) should be located near the *Cpx–Pl* tie-line. However, in actuality, these points group along the *Pl* + *Cpx* + *Ol* eutectic, a fact suggesting that the rocks contain a phase with olivine end-members.

Petrographic observations indicate that the gabbroids originally contained a cumulus silicate mineral (other than plagioclase and clinopyroxene), which is now pseudomorphed by serpentine–chlorite aggregates (Fig. 7). The pseudomorphs are distributed very unequally, their amounts in our thin sections never exceeds 5–8%, and their size varies from 0.2 to 0.6 mm. The pseudomorphs have a short-prismatic, barrel-shaped, or oval habits (Fig. 7), and their cores sometimes bear relics of reticulate textures (which are typical of the initial replacement of olivine by serpentine) but are more often dominated by fibrous aggregates.

Table 1. Chemical and normative compositions (wt %) of the Pilgujarvi intrusions and some petrochemical coefficients

	ca-51	ca-21	ca-4	ca-6	ca-11	ca-5	ca-12	ca-41	ca-158
Component	1	2	3	4	5	6	7	8	9
	5*	33	66	112	136	160	230	272	272
SiO_2	48.10	49.59	48.60	44.26	47.18	45.48	43.94	40.50	43.52
TiO_2	3.59	3.04	2.54	4.69	3.70	4.08	3.26	4.87	3.30
Al_2O_3	13.04	12.84	13.28	12.46	13.18	12.93	14.65	5.89	8.39
Fe_2O_3	1.08	1.57	3.93	3.98	4.70	4.84	4.45	6.96	2.00
FeO	13.87	11.61	9.88	11.54	10.78	10.38	10.38	15.12	11.87
MnO	0.23	0.18	0.21	0.19	0.13	0.12	0.18	0.19	0.30
MgO	4.12	3.76	3.21	6.04	4.38	5.13	5.38	9.27	12.04
CaO	5.72	8.07	8.54	10.10	8.47	11.26	10.92	13.87	12.32
Na_2O	3.29	4.45	3.91	3.30	3.55	2.93	2.76	0.88	0.48
K_2O	2.68	1.62	1.71	0.19	0.85	0.24	0.61	0.36	1.38
H_2O^-	0.20	0.14	0.16	0.08	0.38	0.16	0.10	0.14	0.08
LOI	3.24	2.61	2.50	2.87	2.31	2.01	2.67	1.85	3.93
P_2O_5	–	0.42	1.10	0.18	0.22	0.15	0.11	0.08	0.16
CO_2	0.19	0.13	0.08	0.01	0.08	0.14	0.10	0.09	–
S	0.20	0.20	–	0.21	–	0.20	0.31	0.45	–
Cr_2O_3	–	0.01	–	0.01	0.01	0.02	0.01	–	–
NiO	0.01	–	0.00	–	–	–	–	0.04	0.04
Total	99.56	100.24	99.65	100.11	99.92	100.07	99.83	100.56	99.81
*C*al	0.43	0.30	0.18	0.02	0.18	0.32	0.23	0.20	–
Ap	–	0.99	2.61	0.43	0.52	0.36	0.26	0.19	0.38
Ilm	6.82	5.78	4.83	8.91	7.03	7.75	6.20	9.25	6.27
Mag	1.57	2.28	5.70	5.77	6.82	7.02	6.45	10.10	2.90
Hem									
Chr	–	0.01	–	0.01	0.01	0.03	0.01	–	–
Py	0.37	0.37	–	0.39	–	0.37	0.58	0.84	–
Or	15.83	9.57	10.10	1.12	5.02	1.42	3.60	2.13	8.15
Ab	27.82	34.16	3.07	27.31	30.02	24.78	22.16	7.44	4.06
An	12.90	10.28	13.64	18.63	17.52	21.42	25.79	11.06	16.66
Ne	–	1.88	–	0.30	–	–	0.64	–	–
En	1.69	–	2.78	–	5.65	4.65	–	2.12	4.19
Fs	3.08	–	3.86	–	5.20	2.95	–	1.24	2.14
Di	4.65	9.21	7.96	15.59	10.32	17.08	13.57	30.53	24.32
Hd	7.39	12.79	9.63	9.10	8.28	9.47	8.58	15.54	10.84
Fo	4.49	3.57	1.06	5.47	0.33	0.14	4.98	4.77	10.17
Fa	9.01	6.27	1.63	4.04	0.33	0.10	3.97	3.07	5.73
An(norm)	30.42	22.10	28.00	39.14	35.49	44.90	52.30	58.34	79.46
F#	66.91	66.03	70.11	58.42	65.79	61.72	60.01	56.42	38.92
Sum(*Fsp*)	65.10	63.71	67.84	58.08	63.58	58.07	62.69	26.49	33.47
K(hy)	28.38	0.00	27.42	0.00	36.85	22.26	0.00	6.78	15.27
f(hy)	58.09	54.80	51.37	33.76	41.19	32.61	35.51	30.76	28.01

Table 1. (Contd.)

Component	ca-7	ca-8	ca-9	ca-19	ca-15	ca-13	ca-34	ca-36	ca-10
	10	11	12	13	14	15	16	17	18
	280	288	292	296	313	313	323	328	340
SiO_2	43.66	42.42	42.68	43.73	36.42	41.32	47.92	45.93	37.06
TiO_2	2.23	3.12	6.14	4.93	5.81	3.68	1.09	1.48	0.85
Al_2O_3	14.64	13.34	12.82	13.49	5.64	7.28	2.88	4.15	3.40
Fe_2O_3	5.56	5.07	2.65	2.62	8.32	5.38	4.74	3.24	9.87
FeO	9.05	10.79	12.20	12.02	16.55	12.06	6.08	10.29	10.12
MnO	0.15	0.18	0.21	0.17	0.23	0.14	0.16	0.20	0.16
MgO	6.15	6.97	6.91	5.71	9.61	9.82	17.17	15.69	26.47
CaO	11.90	11.85	9.80	9.52	13.92	15.71	16.79	15.48	3.11
Na_2O	2.69	1.94	2.90	2.72	0.25	0.96	0.34	0.42	0.19
K_2O	0.37	0.50	0.30	1.33	0.08	0.07	0.08	0.14	0.30
H_2O^-	0.06	–	0.12	0.16	0.09	0.12	0.04	0.16	0.23
LOI	2.98	–	2.72	3.44	2.35	1.96	2.07	2.41	7.47
P_2O_5	0.11	0.07	0.06	0.09	0.05	0.51	0.06	–	0.05
CO_2	0.11	0.04	0.20	0.23	0.04	0.20	–	0.03	0.20
S	0.53	0.17	0.09	–	0.41	0.79	0.34	0.35	0.44
Cr_2O_3	0.02	–	0.01	–	0.02	0.05	0.26	0.20	0.49
NiO	0.00	–	–	0.01	0.02	–	0.04	0.06	0.17
Total	100.21	96.46	99.81	100.17	99.81	100.05	100.06	100.23	100.58
*C*al	0.25	0.09	0.45	0.52	0.09	0.45	–	0.07	0.45
Ap	0.26	0.17	0.14	0.21	0.12	1.21	0.14	–	0.12
Ilm	4.24	5.93	11.67	9.37	11.04	6.99	2.07	2.81	1.62
Mag	8.06	7.35	3.84	3.80	12.07	7.80	6.88	4.70	14.32
Hem									
Chr	0.03	–	0.01	–	0.03	0.07	0.38	0.29	0.72
Py	0.99	0.32	0.17	–	0.77	1.48	0.64	0.65	0.82
Or	2.19	2.95	1.17	7.86	0.47	0.41	0.47	0.83	1.77
Ab	20.06	16.41	23.89	20.73	2.11	8.12	2.88	3.55	1.61
An	26.78	26.22	21.08	20.68	14.03	15.35	6.10	9.03	7.54
Ne	1.46		0.35	1.23					
En	–	0.05	–	–	1.72	1.08	13.01	6.48	24.13
Fs	–	0.03	–	–	0.97	0.45	1.49	2.22	3.04
Di	17.47	17.00	13.85	11.57	29.63	34.24	54.99	41.73	4.47
Hd	7.47	8.93	7.21	8.59	14.60	12.47	5.49	12.44	0.49
Fo	5.05	6.60	7.56	6.20	5.94	5.25	2.97	9.27	27.82
Fa	2.73	4.39	4.97	5.82	3.70	2.42	0.37	3.49	3.86
An(norm)	55.72	60.10	45.41	48.45	86.22	64.05	66.65	70.54	81.56
F#	56.19	55.28	54.22	58.56	58.40	49.13	25.27	32.08	28.72
Sum(*Fsp*)	60.67	55.20	58.37	61.08	22.71	29.93	10.76	15.05	14.61
K(hy)	0.00	0.30	0.00	0.00	5.73	3.17	19.34	13.84	84.55
f(hy)	27.19	31.44	31.24	39.31	30.08	24.13	8.01	20.65	8.74

Table 1. (Contd.)

Component	ca-40	ca-14	ca-78	ca-25	ca-26	ca-29	ca-49	927-2	ca-48
	19	20	21	22	23	24	25	26	27
	351	361	390	390	450	454	462	462	466
SiO_2	36.74	36.81	35.27	34.97	37.39	33.09	42.75	40.56	38.59
TiO_2	0.86	0.81	0.63	1.08	1.29	0.95	1.94	2.48	2.50
Al_2O_3	2.69	2.97	2.24	2.03	4.60	2.26	7.11	7.62	9.50
Fe_2O_3	7.45	5.12	6.57	11.91	8.94	14.05	2.11	1.67	2.14
FeO	11.51	13.26	13.17	11.90	9.12	8.42	13.91	15.24	14.05
MnO	0.23	0.19	0.23	0.20	0.18	0.27	0.20	0.36	0.27
MgO	28.86	30.05	31.70	29.32	23.96	27.47	16.84	16.72	15.72
CaO	2.60	2.02	1.98	1.81	3.94	1.25	8.66	8.08	8.59
Na_2O	0.17	0.14	0.19	0.11	0.34	0.11	0.67	0.14	0.51
K_2O	0.29	0.31	0.25	0.10	0.21	0.10	0.06	0.03	0.08
H_2O^-	0.22	0.18	0.11	–	0.32	0.16	0.18	0.12	0.26
LOI	7.42	6.53	6.32	5.19	7.73	8.91	4.77	5.52	5.91
P_2O_5	0.06	0.05	–	0.04	0.13	0.07	0.19	0.65	0.24
CO_2	0.11	0.13	0.08	0.19	0.86	–	0.04	0.10	1.06
S	0.29	0.39	1.06	0.46	1.33	3.00	–	0.07	–
Cr_2O_3	0.56	0.60	0.50	0.53	0.38	0.43	0.25	–	0.24
NiO	0.24	0.06	0.71	0.20	0.71	0.80	0.20	0.01	0.17
Total	100.30	99.62	101.01	100.04	101.43	101.34	99.88	99.37	99.83
*C*al	0.25	0.30	0.18	0.43	1.96	–	0.09	0.23	2.41
Ap	0.14	0.12	–	0.09	0.31	0.17	0.45	1.54	0.57
Ilm	1.63	1.54	1.20	2.05	2.45	1.81	3.69	4.71	4.75
Mag	10.81	7.43	9.53	17.28	12.97	16.26	3.06	2.42	3.10
Hem	–	–	–	–	–	2.84	–	–	–
Chr	0.82	0.88	0.74	0.78	0.56	0.63	0.37		0.35
Py	0.54	0.73	1.98	0.86	2.49	5.61	–	0.13	–
Or	1.71	1.83	1.48	0.59	1.24	0.59	0.35	0.18	0.47
Ab	1.44	1.18	1.61	0.93	2.88	0.93	5.67	1.18	4.31
An	5.72	6.56	4.52	4.75	10.41	5.38	16.22	20.07	23.40
Ne									
En	16.61	13.48	6.54	21.25	31.25	30.64	14.74	19.66	12.66
Fs	3.08	3.23	1.39	2.78	3.01	–	7.42	10.89	6.63
Di	4.15	1.52	3.21	1.96	2.07	0.28	14.21	8.28	6.09
Hd	0.67	0.32	0.60	0.22	0.17	–	6.23	4.00	2.78
Fo	37.36	42.48	49.67	35.62	19.22	26.36	14.43	12.70	16.57
Fa	7.64	11.21	11.64	5.13	2.04		8.01	7.75	9.57
An(norm)	79.00	83.93	72.62	82.80	77.33	84.49	72.95	94.11	83.64
F#	26.16	25.02	25.25	30.21	28.68	30.09	34.51	35.98	36.32
Sum(*Fsp*)	11.32	11.70	9.43	8.56	20.09	10.75	25.48	25.30	34.17
K(hy)	80.32	90.09	67.57	91.68	93.86	99.08	52.02	71.33	68.50
f(hy)	12.37	15.42	13.93	9.05	6.84	0.00	27.70	29.65	28.50

Note: (1–13) Gabbro zone, (14–17) clinopyroxenite zone, (18–27) wehrlite zone. Sum(*Fsp*) = *Ab* + *Or* + *An*; *An*(norm) = 100 × *An*/(*An* + *Ab*); *F*# = 100 × (Fe^{2+} + Fe^{3+})/(Fe^{2+} + Fe^{3+} + Mg); *K*(hy) = 100 × *Opx*/(*Opx* + *Cpx*); *f*(hy) = 100 × *Fs*/(*Fs* + *En*), LOI is loss on ignition. Analyses were conducted by atomic absorption at the Geological Institute, Kola Research Center, Russian Academy of Sciences. Dashes denote element concentrations <0.01 wt %.

*Depth, m.

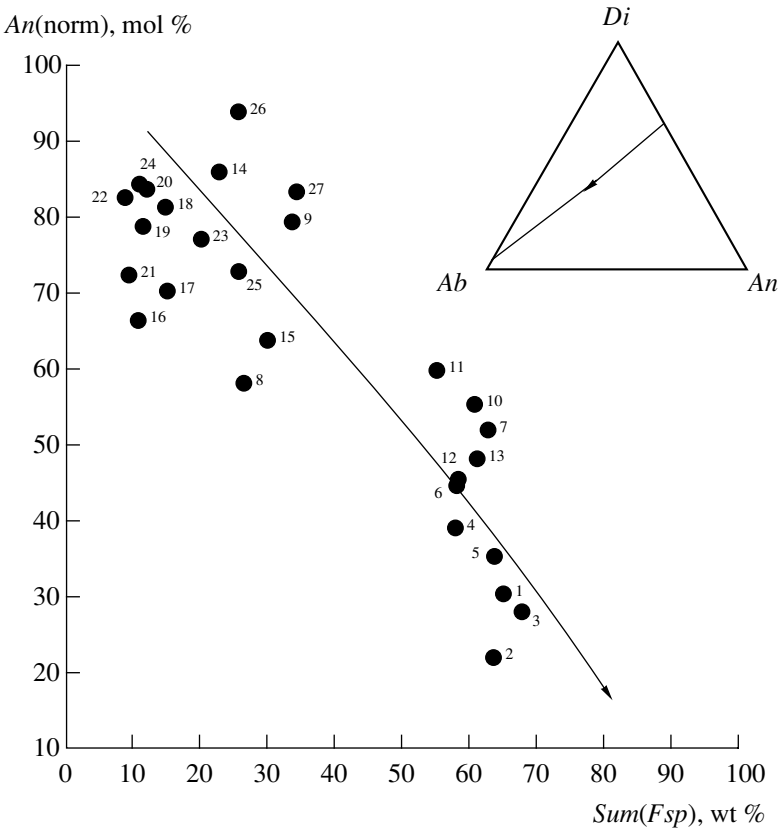

Fig. 5. *An*(norm)–Sum(*Fsp*) plot for the composition of rocks of the Pilgujarvi intrusion. *An*(norm) = 100 × *An*/(*An* + *Ab*), Sum(*Fsp*) = *Ab* + *Or* + *An*.

The *An–Ab–Di* triangular plot illustrates the variations in the modal proportions of plagioclase and clinopyroxene on the cotectic line in the course of differentiation. Based on the petrochemical diagram designed by Dubrovskii (1998).

The structures, fabrics, and composition of these pseudomorphs are very similar to those of pseudomorphs after olivine in the wehrlites in the lower part of the intrusion. This led us to hypothesize that the gabbroids had contained primary olivine. Thus, the passage from the transitional unit to the gabbro zone was not associated with the termination of olivine crystallization, and the rocks of the latter zone correspond to olivine–clinopyroxene–plagioclase (but not clinopyroxene–plagioclase) cumulates. Hence, the actual trend of the Pechenga Ni-bearing intrusions corresponded to one of the theoretically permitted crystallization trends of mafic magmas: $Ol \longrightarrow Ol + Cpx \longrightarrow Ol + Cpx + Pl$ (Irvine, 1970).

Estimation of the Correctness of the Primary Melt Compositions Proposed for the Pechenga Gabbro–Wehrlite Intrusions

During the long-term studies of the Pechenga Ni-bearing intrusions, many attempts were undertaken to reproduce the composition of the primary melts (Eliseev *et al.*, 1961; Predovskii *et al.*, 1971; Zhangurov and Predovskii, 1974; Smolkin, 1974, 1977a, 1999; Lyakhnitskaya *et al.*, 1980; *Magmatizm…*, 1995; and others). The very first reconstructions (accomplished in the 1960s) were based on the then-prevailing idea of the tholeiitic composition of sulfide-bearing magmas. Proceeding from the finding of picritic volcanics in the upper portion of the Pechenga structure, Predovskii *et al.* (1971) put forth an idea of the picritic composition of these magmas. This concept was further developed by Smolkin (1974–1999). The metalliferous magmas intruded into the Pechenga structure were specific in their enrichment not only in Mg and Ni but also in Ti, P, and REE, which provided grounds for the classification of the melts with the ferropicritic type (Smolkin, 1992; Hanski, 1992). The intrusion of ferropicritic magmas was associated with a wide spectrum of comagmatic phenomena (gabbro–wehrlite intrusions, ferropicrite volcanics, and dikes of ferrodolerite, peridotite, and olivine gabbro), which composed a volcanoplutonic association (Smolkin, 1992; *Mednonikelevye…*, 1999).

The composition of the parental melts of the Pechenga intrusion was calculated from different premises: the weighted mean compositions of individual intrusions or all exposed intrusions; the averaged composi-